Crystallization kinetics of Al 2 O 3 -28mol%Lu 2 O 3 glass and full crystallized transparent Lu 3 Al 5 O 12 -based nanoceramics

Jie Fu, Ying Zhang, Zhibiao Ma, Linghan Bai, Ruyu Fan, Wenlong Xu, Mathieu Allix, Cécile Genevois, Emmanuel Veron, Yafeng Yang, et al.

Crystallization kinetics of Al_2O_3-28mol%Lu_2O_3 glass and full crystallized transparent $Lu_3Al_5O_{12}$-based nanoceramics

Jie Fu[a,b,d], Ying Zhang[a,d], Zhibiao Ma[b], Wenlong Xu[b], Mathieu Allix[c], Cécile Genevois[c], Emmanuel Veron[c], Linghan Bai[b], Ruyu Fan[b], Hui Wang[a,d], and Jianqiang Li[a,b,d,*]

[a]*State Key Laboratory of Multiphase Complex Systems, Institute of Process Engineering, Chinese Academy of Sciences, Beijing 100190, China*

[b]*School of Materials Science and Engineering, University of Science and Technology Beijing, Beijing 100083, PR China*

[c]*CNRS, CEMHTI UPR 3079, Univ. Orléans, 45071 Orléans, France*

[d]*University of Chinese Academy of Sciences, Beijing 100049, China*

Abstract

Transparent $Lu_3Al_5O_{12}$ (LuAG) ceramics have become very promising phosphor matrix materials due to their high doping concentration and luminous efficiency, thermal conductivity and thermal stability. However, LuAG transparent ceramics prepared by traditional powder sintering method are facing several problems, such as time-consuming and energy-consuming, complex preparation process, high purity of raw material powders and large crystalline grain size. Here we report facile elaboration of transparent LuAG-Al_2O_3 two-phase nanocrystalline ceramics through pressureless crystallization (1000 ℃, 2 h) of 72 mol.% Al_2O_3-28 mol.% Lu_2O_3 (ALu28) bulk glasses combined with the crystallization kinetics analysis. The results of the crystallization kinetics analysis show that the ALu28 bulk glasses have a low activation energy (<750 kJ·mol^{-1}) and a crystallization mechanism of three-dimensional crystal growth mode accompanied by volume nucleation. The resulting LuAG-Al_2O_3 ceramics with nanosized grains and dense three-dimensional network nanostructures present good transmittance (80.6%@780 nm) and excellent mechanical properties (hardness is 24 GPa).

Keywords: Transparent LuAG-Al_2O_3 nanoceramics, LuAG glass, Crystallization kinetics

1. Introduction

The advancement of solid-state lighting (SSL) technology[1-3] on the basis of light-emitting diodes (LED)[4-6] and laser diodes (LD)[7-9] has brought about great changes in the field of lighting. Compared with traditional light sources, SSL devices have the advantages of compact structure, high luminous efficiency, long life, energy conservation and the "intelligent" controllability of

spectrum, color temperature, and spatial distribution. Therefore, SSL technology has great application prospects in lighting, automotive, imaging and other fields.[10] With the continuous breakthrough of blue LED and blue laser diode (LD) technology, higher requirements have been put forward for the performance of phosphor materials.[8,11] Compared with Ce:$Y_3Al_5O_{12}$ (Ce:YAG) phosphor ceramics which have been widely studied,[12-16] Ce:LuAG phosphor ceramics demonstrate higher luminous efficiency, better thermal quenching temperature and quantum efficiency, and become a hot research material of SSL.[16-20] Ma et al.[21] successfully prepared LuAG transparent ceramics with different Ce^{3+} doping concentrations by vacuum sintering. The Ce:LuAG transparent ceramic emits yellow-green light when combined with LED chip, its luminous efficiency is up to 223.4 $lm \cdot W^{-1}$, and the maximum color rendering index is 55.8. Xu et al.[22] synthesized Ce:LuAG translucent phosphor ceramics by spark plasma sintering (SPS) technology. The obtained phosphor ceramics have external quantum efficiency (up to 77%), good thermal conductivity (6.3 $W \cdot m^{-1} \cdot K^{-1}$) and high reliability (98.1% luminescence intensity after 1000 h, at 85 C and 85% humidity). Zhang et al.[23] also prepared Ce:LuAG phosphor ceramics at high temperature. The phosphor ceramics show good thermal stability (90% PL intensity at 450 K) and high luminous efficiency (200 $lm.W^{-1}$). However, the above sintering methods such as vacuum sintering[24-25], hot isostatic pressing sintering[26-27] and spark plasma sintering [22] require high temperature, high pressure and high purity raw material powder which makes the preparation of transparent Ce:LuAG ceramics through the above sintering methods complex and difficult. The grains of the obtained ceramics are micron or submicron scale, some pores and second phases are also formed.[23] These factors can cause strong scattering effect and make it difficult to prepare transparent ceramics with high transmittance by above traditional sintering method. Therefore, there is an urgent need for a novel preparation method with lower temperature and simpler process to synthesize transparent ceramics.

Glass-crystallization technology is a promising ceramic preparation technology emerging in recent years, which is a process of amorphous glass materials are heat-treated at an appropriate temperature (≤1200 ℃) and then transformed into ceramic materials in a relatively short time (<10 h).[28] Rosenflanz et al.[29] heat-treated Al_2O_3-ZrO_2-Re_2O_3 (Re=La, Gd, Y) bulk glass material, and successfully obtained a highly transparent and ultrahard transparent ceramic material with nano sized grains. The research on the preparation of transparent ceramics by glass-crystallization has

attracted great attention, and this method making it possible to prepare transparent ceramics in the middle temperature region (≤1200 ℃). Allix et al. have prepared a variety of transparent ceramics with excellent performance through glass-crystallization method, including $BaAl_4O_7$,[30] $Sr_3Al_2O_6$[31] and $Sr_{1+x/2}Al_{2+x}Si_{2-x}O_8$ ($0<x\leqslant 0.4$)[32]. And in our recent work, Al_2O_3-Y_2O_3 glass obtained by containerless solidification process was successfully crystallized to fully dense YAG nanocrystalline ceramics with high transmittance.[33] However, up to now LuAG transparent ceramics with nanosized grains have been rarely reported, and much less by glass crystallization method. Therefore, full crystallization from glass can be a suitable route to obtain LuAG-based transparent nanoceramics.

It is of great significance to study the crystallization kinetics of glass to better control the process of glass crystallization. For decades, researchers have conducted in-depth researches on the crystallization mechanism of garnet series glasses, but mainly for opaque polycrystalline ceramics with micron or submicron grains[34-36]. However, there are few reports on the crystallization mechanism of glass which is crystallized into transparent polycrystalline ceramics with nanocrystalline. In our recently previous work, a transparent YAG-Al_2O_3 nanoceramic material with better performance was obtained through the analysis of crystallization kinetics of AY26 glass.[37] In this work, the non-isothermal thermal analysis is used to analyze the crystallization kinetics of Lu_2O_3-Al_2O_3 glass, and the Kissinger,[38] Augis-Bennett and Ozawa models[39-40] are the main theoretical analysis models. Afterwards, LuAG-Al_2O_3 transparent nanoceramics were prepared by glass crystallization method. The crystalline phase, microstructure, in-line transmittance and mechanical properties of LuAG-Al_2O_3 transparent nanoceramics were systematically investigated and analyzed.

2. Experimental procedure

2.1. Preparation of ALu28 glass and LuAG-Al_2O_3 transparent ceramics

Commercial oxide powders Al_2O_3 (99.99%, Aladdin Reagent (Shanghai) Co., Ltd., China), and Lu_2O_3 (99.99%, Beijing Hulk Technology Co., Ltd., China) were used as starting materials. Our previous work on $Lu_3Al_5O_{12}$-Al_2O_3 transparent nanoceramics revealed that the nanoceramics achieve the highest transmittance when the Lu_2O_3 content is 28%. Therefore, the powders were weighed according to the composition of 72 mol.% Al_2O_3-28 mol.% Lu_2O_3, and were ground and mixed uniformly in a corundum mortar with absolute ethanol as a solvent. The powders were dried

in an air drying oven at 50 ℃ for 2 h, taken out and compressed into pellets using a powder tablet molding machine. The pellets were broken apart, and 0.05-0.2 g fragments were taken into the aerodynamic levitation furnace coupled with CO_2 laser heating system. The fragments were suspended using oxygen and heated to 2700-2800 ℃ with the laser heating system. Once melted, the fragments were spherical and held at high temperature for 1 minute. The molten materials were subsequently rapidly cooled to room temperature at a cooling rate of 250 °C/s by shutting off the laser, and finally transparent glass beads (with a diameter of 3-5 mm) were prepared. Referring to our previous works, the glass beads were placed in a muffle furnace, heated to 1000 °C at 10 °C/s in an air environment, and kept for 2 h to finally prepare transparent ceramics.

2.2. Characterization

Thermal properties of as-prepared ALu28 glass beads and powders were tested by differential scanning calorimeter (DSC, STA 449F3, NETZSCH, Germany) from room temperature to 1200 ^{o}C, and argon was used as the purging gas. The phase structure and grain sizes of samples were identified by X-ray powder diffraction (XRD, Smartlab 9, Rigaku Corporation, Japan) with Cu-Ka radiation. The density test was completed with the density test system of Mettler Toledo ME204 electronic balance, and the dimension of test samples was Φ3 mm*1 mm. The nanostructures of ceramic materials were observed with transmission electron microscope (TEM, JEM ARM200 F, JEOL, Japan). The in-line transmittance of samples was measured by a UV–Vis-NIR spectrophotometer (Cary 5000, Varian, America). The hardness and Young's modulus of the ceramic samples were measured by nanoindenter (G200, Keysight Technology) with a force of 350 mN and a displacement of 1000 nm and eight indentations were made at least for each sample.

3. Results and discussion

3.1. Crystallization kinetics analysis of ALu28 glass

Non-isothermal thermal analysis is a fast and simple method to study the crystallization kinetics of glass[41-42]. Kissinger, Augis-Bennett and Ozawa's empirical models are commonly used. Through the analysis of crystallization kinetics, the activation energy (E_a) of the crystallization process, the Avrami parameter (n) of crystallization nucleation and the dimensional parameter (m) of crystal growth can be obtained. The activation energy (E_a) reflects the sensitivity of the glass to temperature changes and the difficulty of glass crystallization, while the Avrami parameter (n) and dimensional parameter (m) mainly reflect the crystallization mechanism of glass[43].

The crystallization kinetics and crystallization mechanism of ALu28 bulk glass are analyzed in detail in this work and the results are compared with previous work of AY26 bulk glass. DSC tests performed at different heating rates (β = 5, 10, 20 and 40 °C·min^{-1}) with ALu28 glass beads (3.0 mm in diameter), and the DSC curves are shown in **Figure 1**. The results show that there are obvious exothermic peaks in the DSC curves of ALu28 glass beads at different heating rates, and these exothermic peaks correspond to the crystallization of the LuAG phase. In addition, it can be seen that under non-isothermal conditions, the peak crystallization temperatures (T_p) are 937 °C, 949 °C, 957 °C and 972 °C when the heating rate is 5, 10, 20 and 40 °C·min^{-1}, respectively. Through the Kissinger, Augis-Bennett and Ozawa empirical model, the crystallization activation energy (E_a) of ALu28 glass can be estimated with the peak crystallization temperature (T_p) and the corresponding heating rate[39-40].

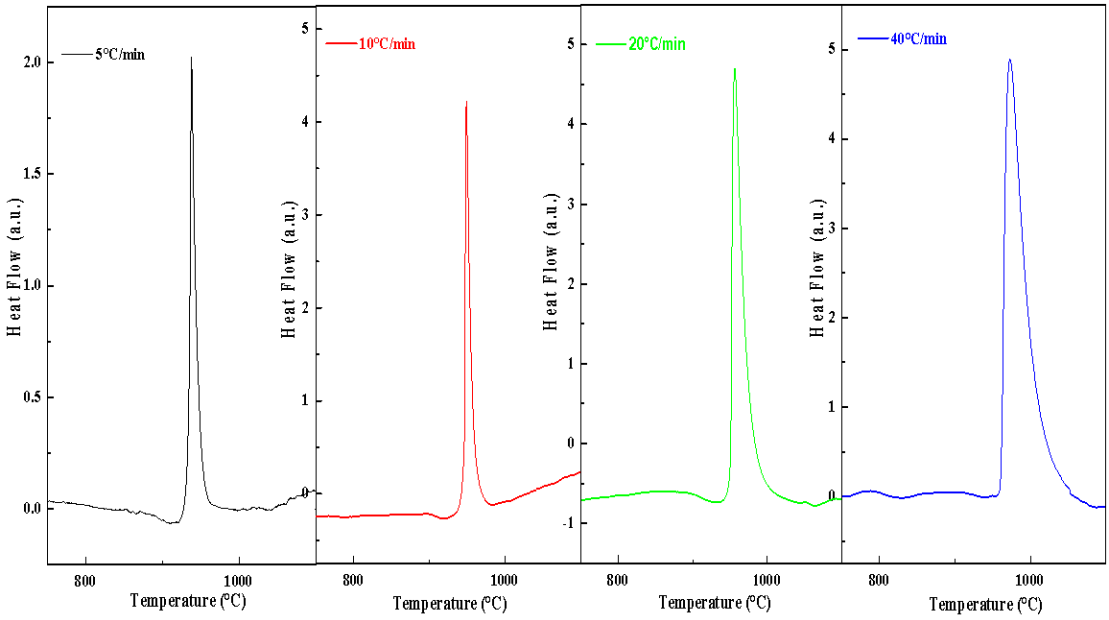

Figure 1. DSC curves of unbroken ALu28 glass beads (3.0 mm) at different heating rates of 5, 10, 20, and 40 °C·min^{-1}.

The Kissinger empirical model, which takes into account the dependence of the peak crystallization temperature (T_p) on the heating rate, has been widely used to calculate the activation energy (E_a) with the following formulae[38]:

$$ln(\frac{\beta}{T_p{}^2}) = -\frac{E_a}{RT_p} + const$$

where β is the heating rate, T_p is the peak crystallization temperature, and R is the ideal gas

constant. Another model proposed by Augis and Bennett[44] is shown as follows:

$$ln(\frac{\beta}{T_p - T_0}) = -\frac{E_a}{RT_p} + lnK_o$$

where T_0 is usually 300 K, and K_0 is the frequency factor. Finally, Ozawa believes that the degree of reaction is constant and independent of the heating rate, and proposes Ozawa model which is given in the following equation[45]:

$$ln\,\beta = -\frac{E_a}{RT_p} + const$$

Figure 2(a) is the fitted straight line between $ln\,(\beta/(T_p - T_0)^n)$ and $(1000/T_p)$, where n = 2, 1, 0, and corresponding to the Kissinger, Augis-Bennett and Ozawa models, respectively. For the Kissinger and Ozawa models, T_0 = 0 K, and for the Augis-Bennett model, T_0 = 300 K. The activation energies (E_a) calculated from the slopes of the fitted straight lines obtained from the Kissinger, Augis-Bennett and Ozawa models were 728.0, 734.9 and 748.7 kJ·mol^{-1}, respectively. It can be seen that the activation energy (E_a) values of the ALu28 bulk glass obtained from these three models are very close and much lower than that of AY26 bulk glass (1535, 1541 and 1556 kJ·mol^{-1})[37]. Therefore, compared with AY26 glass, ALu28 glass has a lower thermal stability and is more likely to crystallize through heat treatment to prepare transparent nanoceramics.

The Avrami parameter (n) is related to the crystallization mechanism and can be determined according to the following formula[46]:

$$\left.\frac{dln[-ln(1-x)]}{d\,ln\,\beta}\right|_{T_y} = -n$$

where x is the volume fraction of the crystalline phase at a given temperature T_y. The linear fit of $ln[-ln(1-x)]$ with $ln\,\beta$ is shown in **Figure 2(b)**. The Avrami parameter n = 2.68 was calculated from the slope of the fitted straight line, which indicates that the nucleation mode of ALu28 glass during crystallization is bulk nucleation. In addition, the Avrami parameter (n) is related to the dimension (m) of crystal growth, which can be calculated by the modified formula of Matussita and Sakka[47]:

$$ln(\frac{\beta^n}{{T_p}^2}) = -\frac{mE_a}{RT_p} + const$$

Among them, the activation energy (E_a) determined according to the Kissinger model was 728.0 kJ·mol^{-1}, and n was 2.68. The fitted straight line between $ln\,(\beta^n/{T_p}^2)$ and $(1000/T_p)$ is

shown in **Figure 2(c)**. Finally, m = 2.73 was calculated from the slope of the fitted straight line, which implies the mode of three-dimensional crystal growth. Therefore, the crystallization mechanism of ALu28 glass is a three-dimensional crystal growth mode accompanied by volumetric nucleation.

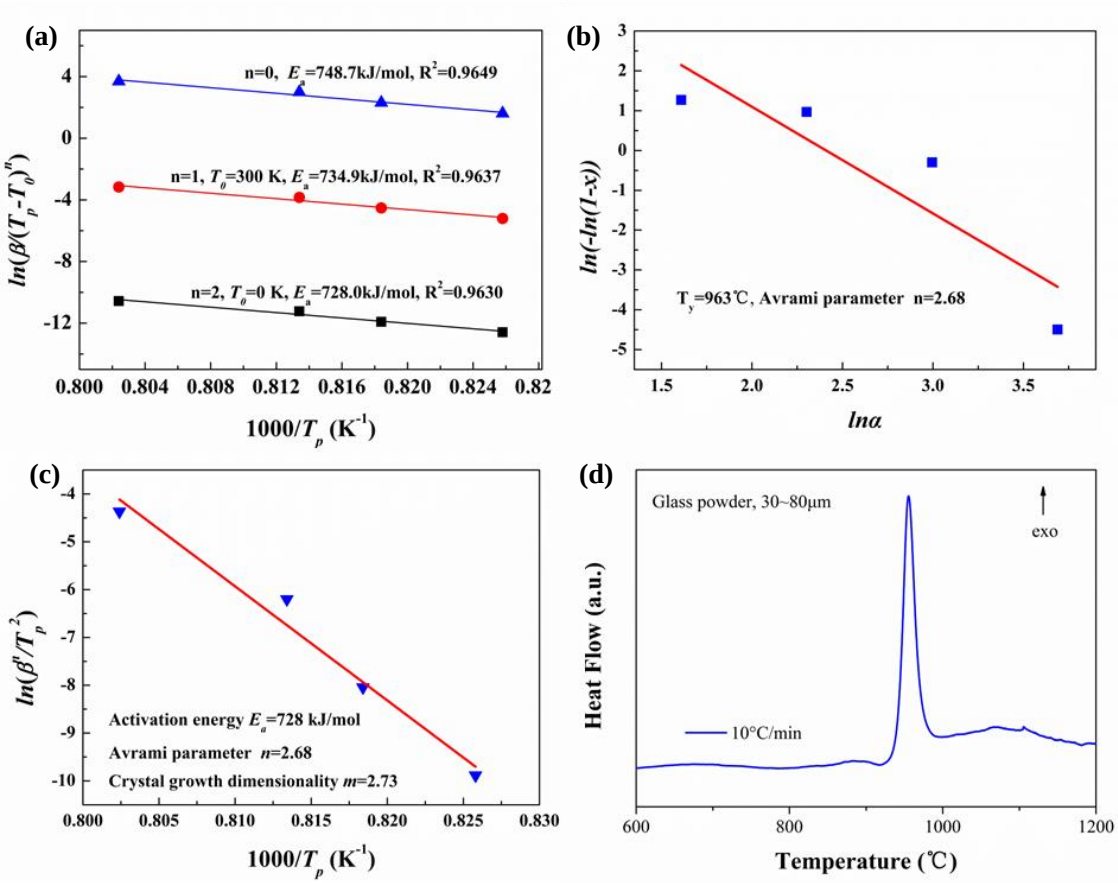

Figure 2. (a) Plots of $ln(\beta/(T_p-T_0)^n)$ vs $(1000/T_p)$, (b) plots of $ln[-ln(1-x)]$ vs $ln\beta$, and (c) plots of $ln(\beta^n/T_p^2)$ vs $(1000/T_p)$, (d) DSC curve of ALu28 glass powder (30~80 μm) under constant heating rate of 10 °C·min^{-1}.

To further verify the crystallization behavior of ALu28 bulk glass samples, ALu28 glass beads were broken and ground into glass powder with a particle size of 20-90 μm. Then, the DSC test was carried out at a heating rate of 10 °C·min^{-1} to observe the thermal behavior of the ALu28 glass powder. Kalyandurg et al.[48] found that when the crystal growth mechanism of glass during crystallization is controlled by the surface, the thermal behavior of glass powder is significantly different from that of bulk glass, thus showing different endothermic/exothermic phenomena on the DSC curves. However, it can be seen from **Figure 2(d)** that the DSC curve of the ALu28 glass powder is almost consistent with that of the ALu28 glass bead, which indicates that the

crystallization behavior of the ALu28 glass powder and glass bead is same, and further proves that the crystal growth mechanism of the ALu28 glass is the volumetric control. The three-dimensional crystal growth mode is more conducive to the release of shrinkage stress during the crystallization process and enable to obtain completely dense nanoceramic materials. Zhang et al.[37] found that a lower heating rate is more conducive to ensure that the glass sample remains transparent after crystallization. When the heating rate is too high (exceed 20 ℃/s), the glass is more likely to become opaque during crystallization. Therefore, through proper heat treatment, ALu28 glass is likely to crystallize into transparent nanoceramics.

3.2. Preparation of transparent LuAG-Al_2O_3 nanoceramics

According to the above analysis of crystallization kinetics of ALu28 glass, a heat treatment temperature (1000 ℃) slightly higher than the peak crystallization temperature (T_p=949 ℃) and a heating rate of 10 ℃/s were used to crystallize the ALu28 bulk glasses for different times to obtain transparent LuAG-Al_2O_3 nanoceramic materials. **Figure 3(a-b)** show the XRPD patterns of ceramic samples obtained from ALu28 bulk glasses crystallized at 1000 ℃ for different times. The results show that when the crystallization time is 0.17 h (10 min), the $Lu_3Al_5O_{12}$ crystal phase is basically formed, and the other crystal phases cannot be detected. But the Al_2O_3 crystal phase is found in the high-resolution XRPD pattern of ceramic sample obtained from ALu28 bulk glass crystallized at 1000 ℃ for 2 h (**Figure S1**), which is also confirmed by the TEM images of this ceramic sample (**Figure 4**). With the prolongation of crystallization time, the diffraction peaks of $Lu_3Al_5O_{12}$ phase in the obtained ceramic samples were gradually enhanced. When the crystallization time reached 72 h, no other crystalline phases were found in the obtained ceramic samples. When the effect of stress is considered, the Scherrer formula[49] is used to calculate the grain size of the ceramic samples obtained by crystallization at 1000 ℃ for 0.17~72 h, as shown in **Figure 3(c)**. The results show that with the prolongation of crystallization time, the grain size of the obtained ceramic samples increases gradually. When the crystallization time reaches 72 h, the grain size is still in the nanoscale, and unexceed 50 nm. It shows that the grain size of the obtained ceramic samples increases with the prolongation of crystallization time, but the growth rate is very slow, this is mainly due to the existence of Al_2O_3 second phase which limits the excessive growth of LuAG grains. **Figure 3(d)** shows the densities of ALu28 glass and ceramic samples crystallized from ALu28 glasses at 1000 ℃ for different times. The density of ALu28 glass is 5.7g·cm^{-3} and the

ceramic sample obtained by crystallization for 120 min (2 h) has a density of 6.25 g·cm^{-3}, there is a volume shrinkage of about 9.6% here. When the crystallization time exceeds 2 h, the density of the obtained ceramic samples almost no longer changes, indicating that the volume shrinkage is complete. These results indicate that the ALu28 glass-based precursor can be completely crystallized within 2 h, and further extension of the crystallization time cannot lead to the change of phase in the nanoceramic material.

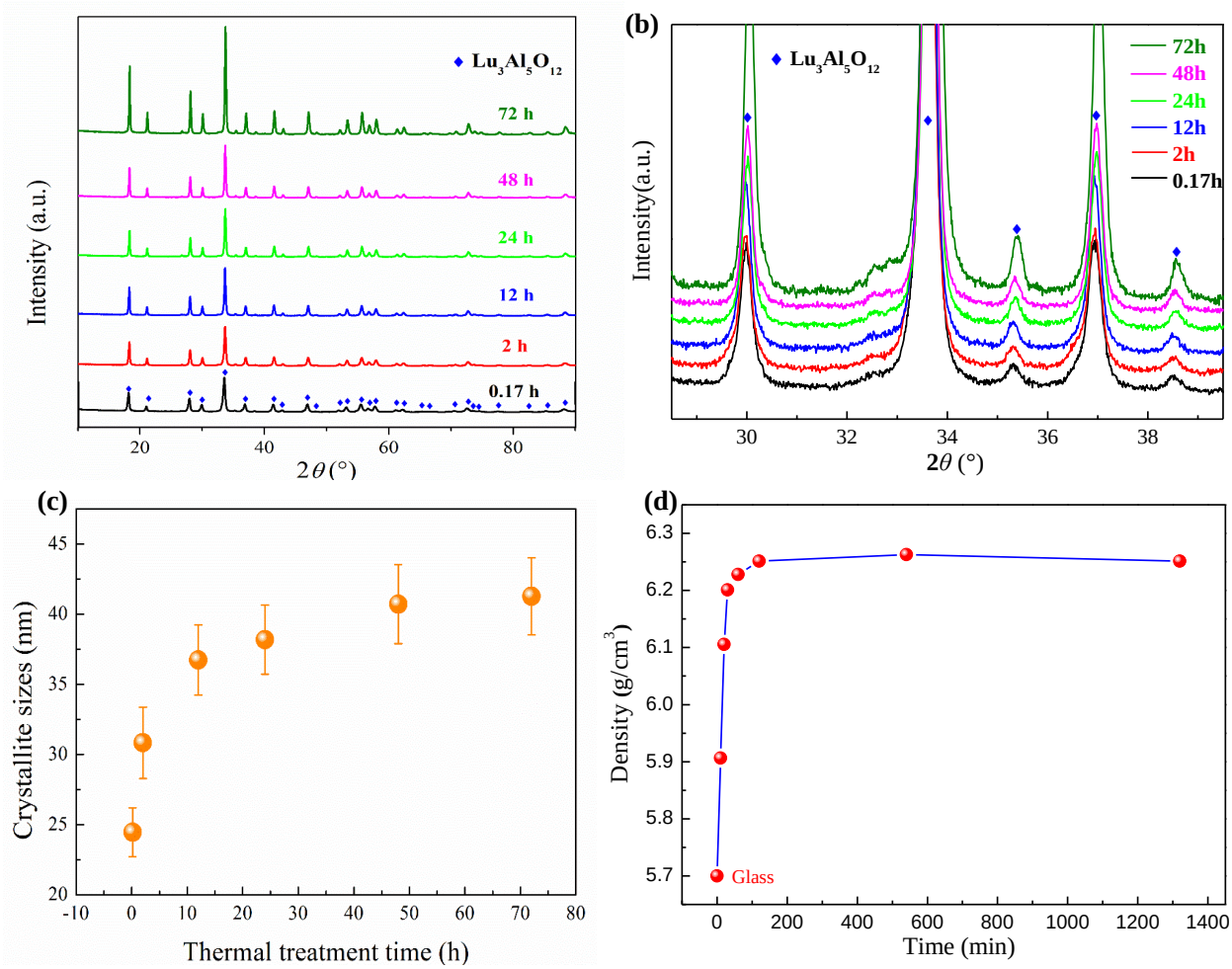

Figure 3. (a-b) The XRPD patterns, (c) crystallite sizes, and (d) densities of ALu28 glass and ceramic samples crystallized from ALu28 glasses at 1000 ℃ for different times.

Figure 4 shows the TEM micrographs of transparent LuAG-Al_2O_3 nanoceramic crystallized from ALu28 glass at 1000 ℃ for 2 h. **Figure 4(a)** is the TEM image of transparent LuAG-Al_2O_3 nanoceramic, from which it can be seen that there are two different grain phases (LuAG and Al_2O_3). The grains of LuAG appear in continuous uniform region and the alumina ones in multiparticulate region. The grain size of LuAG grain phase is below 50 nm. There are two different populations for the alumina grains, big ones which are interconnected with an average

size of 18-20 nm and individual small spherical ones with an average diameter of around 6-7 nm, which can also be seen from the HRTEM image of transparent LuAG-Al_2O_3 nanoceramic (**Figure 4(b)**). The larger alumina grains are located at LuAG grain boundaries (intergranular) and accommodate the LuAG grain organization, which explains their shapes of hills. The smaller spherical grains are situated within LuAG grains (intragranular). For the smaller spherical alumina grains, it is also possible to observe the continuity of the LuAG network around the particle of alumina by HRTEM image in **Figure 4(b)**. **Figure 4(c)** is the HAADF-HRSTEM micrograph and EDX line-scan results of transparent LuAG-Al_2O_3 nanoceramic. It can be seen that the Al element in the dark area accounts for nearly 100%, while the Al and Lu elements in the bright area account for about 60% and 40%, respectively, which is consistent with the atomic ratio of Al element (62.5%) and Lu element (37.5%) in the LuAG ($Lu_3Al_5O_{12}$) phase. It is obvious that the dark area is Al_2O_3, and the bright area corresponds to LuAG. **Figure 4(d)** is HRTEM micrograph of **Figure 4(c)** and the insets in **Figure 4(d)** are the Fourier transformation diffractograms of the selected areas indicated by squares. From the **Figure 4(d),** it can be clearly observed that the circular area is the Al_2O_3 phase, and the surrounding continuous area is the LuAG phase. Therefore, it can be found that the transparent LuAG-Al_2O_3 nanoceramic forms a three-dimensional network nanostructure in which the Al_2O_3 crystal phase surrounds the LuAG crystal phase. It is the existence of the Al_2O_3 phase that effectively releases the shrinkage stress and avoids the generation of microcracks and micropores. Even if a huge volume shrinkage occurs, a fully dense nanoceramic structure can still be obtained. At the same time, the existence of Al_2O_3 phase also limits the excessive growth of LuAG grain, so that its grain size can be kept below 50 nm, thus ensuring the high transmittance of LuAG-Al_2O_3 nanoceramics.

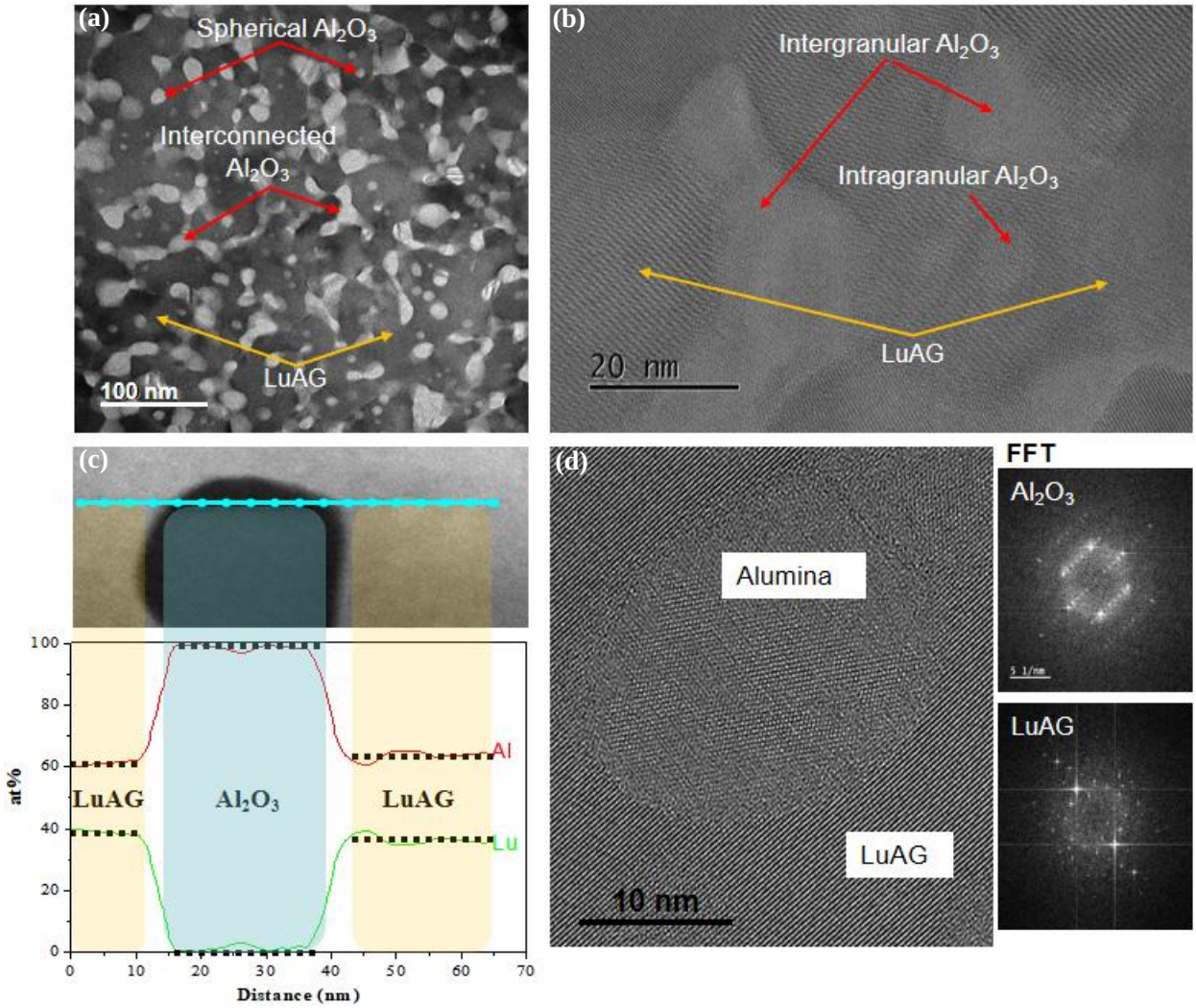

Figure 4. (a) TEM image, (b) HRTEM image, (c) HAADF-HRSTEM micrograph and EDX line-scan results, (d) HRTEM micrograph and FFT patterns of transparent LuAG-Al_2O_3 nanoceramic crystallized from ALu28 glass at 1000 ℃ for 2 h.

Figure 5 is the in-line transmittance measured through 1.0 mm thick samples in UV-Vis-NIR light of the transparent LuAG-Al_2O_3 nanoceramics crystallized from ALu28 bulk glass-based precursors at 1000 ℃ for different crystallization times. The photograph of transparent LuAG-Al_2O_3 nanoceramic crystallized at 1000 ℃ for 2 h is embedded and exhibits high transmittance. The results show that the transmittance in visible light band of the obtained transparent LuAG-Al_2O_3 nanoceramics gradually decreases with the prolongation of crystallization time. Combined with the results of the grain size in **Figure 3(c)**, this further suggests that an increase in grain size will lead to a decrease in the transmittance of the transparent LuAG-Al_2O_3 nanoceramics. It is worth noting that the transmittance is almost the same in the wavelength range of 350-780 nm when the crystallization time is 0.17 h and 2 h, and the in-line transmittance reaches 80.6%@780

nm. It can also be seen from **Figure 3(c)** that the grain size of the ceramics obtained with crystallization time of 0.17 h and 2 h are 24 nm and 30 nm, respectively. According to the Rayleigh scattering theory, the difference in their grain size has little effect on the scattering of light in the wavelength range of 350-780 nm, resulting in almost the same transmittance. In the ultraviolet band, since the wavelength of the incident light is shorter, the larger crystal grains are closer to the wavelength of the ultraviolet light, the scattering effect is enhanced. Therefore, the transmittance of the transparent LuAG-Al_2O_3 nanoceramic obtained by crystallization for 2 h is slightly lower than that of 0.17 h in the wavelength below 350 nm.

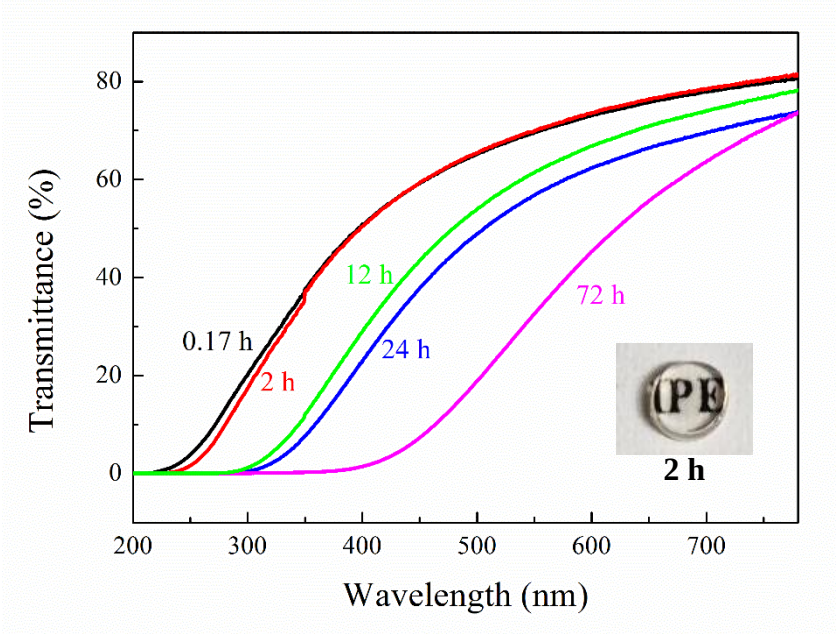

Figure 5. In-line transmittance of transparent LuAG-Al_2O_3 nanoceramics crystallized from ALu28 glass at 1000 ℃ for different crystallization times (0.17 h, 2 h, 12 h, 24 h, 72 h). The photograph of transparent LuAG-Al_2O_3 nanoceramic (2 h) is embedded.

Figure 6 shows the typical load-displacement curves, the hardness and Young's modulus of transparent LuAG-Al_2O_3 nanoceramics obtained by crystallization of ALu28 bulk glass-based precursors at 1000 °C for different times. As shown in **Figure 6(a)**, the load on the LuAG-Al_2O_3 nanoceramic samples surface increases with the indentation depth of the diamond indenter and the load-displacement curves of different crystallization times are very similar. Combining the load-displacement data in **Figure 6(a)** with the Oliver-Pharr model[50], the hardness and Young's modulus of the LuAG-Al_2O_3 nanoceramic samples can be calculated, as shown in **Figure 6(b)**. The results show that the hardness and Young's modulus of the LuAG-Al_2O_3 nanoceramic samples increase gradually with the prolongation of crystallization time, which is because the prolongation

of crystallization time makes the growth of LuAG and Al_2O_3 crystals in the ceramics more perfect, thereby making the mechanical properties of LuAG-Al_2O_3 nanoceramic gradually strengthened. The hardness and Young's modulus of the LuAG-Al_2O_3 nanoceramic obtained by crystallization at 1000 °C for 48 h reached the maximum, which were 24.9 GPa and 330.5 GPa, respectively. However, after the crystallization time exceeds 48 h, the hardness and Young's modulus of the LuAG-Al_2O_3 nanoceramic begin to decrease. According to the Hall-Petch formula[51], the finer the grains of the polycrystalline material, the higher the strength. Therefore, when the crystallization time exceeds 48 h, the excessive increase of the grain size causes the decrease of the hardness and Young's modulus of the LuAG-Al_2O_3 nanoceramic. And when the crystallization time exceeds 2 h, the hardness and Young's modulus of the samples increase little, but only increase by 4±1%. The hardness and Young's modulus of the LuAG-Al_2O_3 nanoceramic obtained by crystallization at 1000 °C for 2 h are 24 GPa and 318 GPa, respectively, which are higher than those of LuAG single crystal (23.1 GPa and 312 GPa). Therefore, transparent LuAG-Al_2O_3 nanoceramic obtained by crystallization at 1000 °C for 2 h also demonstrate good mechanical properties which make it potentially interesting for various optical applications.

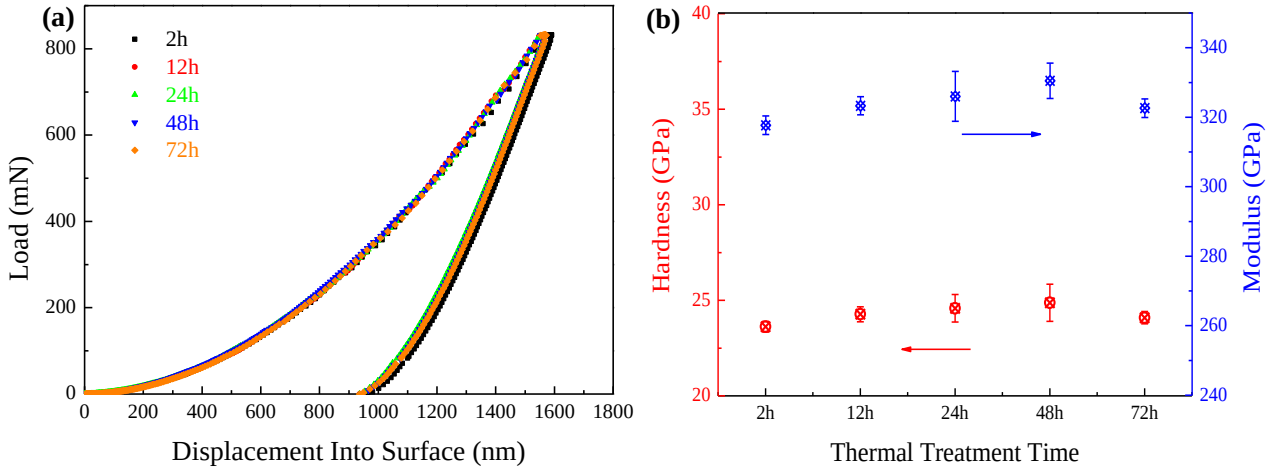

Figure 6. (a) Typical load-displacement curves, (b) hardness and Young's modulus of the transparent LuAG-Al_2O_3 nanoceramics crystallized at 1000 ℃ for different times and YAG single crystal.

4. Conclusion

The crystallization kinetics of ALu28 glass were analyzed, and transparent LuAG-Al_2O_3 nanoceramics were obtained by pressureless crystallization of ALu28 bulk glasses. Crystallization kinetics analysis shows that ALu28 glass has a low activation energy (<750 kJ·mol^{-1}) and a crystallization mechanism of three-dimensional crystal growth mode accompanied by volume

nucleation, which is more conducive to obtain dense ceramic materials. Fully crystallized and dense transparent LuAG-Al_2O_3 nanoceramics were elaborated by heat treatment at 1000 ℃ for 2 h. The obtained transparent LuAG-Al_2O_3 nanoceramics possess nanosized grains (<50 nm) and a three-dimensional network nanostructure of Al_2O_3 crystal phase surrounding LuAG crystal phase was formed. The transparent LuAG-Al_2O_3 nanoceramics have good transmittance in the visible wavelength range (80.6%@780 nm) and excellent mechanical properties (hardness is 24 GPa), which can meet the long-term application requirements in the optical field. The combination of the crystallization kinetics analysis and glass-crystallization method can promote the development of LuAG and other new glass-crystal ceramics applied in the field of optics, such as lenses, scintillators and high-power LED/LD lighting and display.

Declaration of Competing Interest

The authors report no declarations of interest.

Acknowledgement

This work is financially supported by the National Natural Science Foundation of China (NSFC No. 51972304), the Project of Scientific Experiment on Chinese Manned Space Station, Chinese Academy of Sciences President's International Fellowship Initiative for 2021 (No. 2021VEA0012), and the Fundamental Research Funds for the Central Universities. The project benefitted from the microscopy facilities of the Platform MACLE-CVL which was co-funded by the European Union and Center-Val de Loire Region (FEDER).

References

[1] E. F. Schubert, J. K. Kim. Solid-State Light Sources Getting Smart[J]. Science, 2005, 308(5726): 1274-1278.

[2] M. S. Shur, R. Zukauskas. "Solid-State Lighting: Toward superior illumination."[J]. Proceedings of the IEEE, 2005, 93(10): 1691-1703.

[3] J. M. Phillips, M. E. Coltrin, M. H. Crawford, et al. Research challenges to ultra-efficient inorganic solid-state lighting[J]. Laser Photonics Rev, 2007, 1(4): 307-333.

[4] M. H. Crawford. LEDs for solid-state lighting: performance challenges and recent advances[J]. IEEE JOURNAL OF SELECTED TOPICS IN QUANTUM ELECTRONICS, 2009, 15(14):1028-1040.

[5] X. M. Long, J. G. He, J. Zhou, et al. A review on light-emitting diode based automotive headlamps[J]. RENEWABLE & SUSTAINABLE ENERGY REVIEWS, 2015, 41(1): 29-41.

[6] J. M. Li, Z. Q. Liu, T. B. Wei, et al. Development Summary of Semiconductor Lighting in China[J]. Journal Citation Reports, 2021, 41(1): 285-297.

[7] J. C. Camparo. The diode laser in atomic physics[J]. Contemporary Physics, 1985, 26(5): 443-477.

[8] S. X. Li, L. Wang, R. J. Xie, et al. Color Conversion Materials for High-Brightness Laser-Driven Solid-State Lighting[J]. Laser & Photonics Reviews, 2018, 12(12): 1-29.

[9] F. Rahman. Diode laser-excited phosphor-converted light sources: a review[J]. Optical Engineering, 2022, 61(6): 1-16.

[10] J. J. WIERER, J. Y. TSAO, D. S. SIZOV, et al. Comparison between blue lasers and light-emitting diodes for future solid-state lighting[J] Laser & Photonics Reviews, 2013, 7(6): 963-993.

[11] D Chen, W Xiang, X Liang, et al. Advances in transparent glass-ceramic phosphors for white light-emitting diodes-A review[J]. Journal of the European Ceramic Society, 2015, 35(3): 859-869.

[12] G. L. Messing, A. J. Stevenson. Toward pore-free ceramics[J]. Science, 2008, 322(17): 383-384.

[13] R. Won. Ceramic future[J]. Nat. Photonics, 2008, 340(2): 1-2.

[14] H. Wang, Z. Huang, J. Qi, et al. A new methodology to obtain the fracture toughness of YAG transparent ceramics[J]. J. Adv. Ceram, 2019, 8(3): 418-426.

[15] J. Ling, Y. Zhou, W. Xu, et al. Red-emitting YAG:Ce,Mn transparent ceramics for warm WLEDs application[J]. J. Adv. Ceram, 2020, 9 (1): 45-54.

[16] A. C. Berends, M. A. Haar, M. R. Krames. YAG:Ce^{3+} Phosphor: From Micron-Sized Workhorse for General Lighting to a Bright Future on the Nanoscale [J]. 2020, 120(24): 13461-13479.

[17] K. Li, Y. Shi, F. Jia, et al. Low Etendue Yellow-Green Solid-State Light Generation by Laser-

Pumped LuAG:Ce Ceramic[J]. IEEE Photonics Technology Letters, 2018, 30(10): 939-942.

[18] J. Xu, J. Wang, Y. Gong, et al. Investigation of an LuAG:Ce translucent ceramic synthesized via spark plasma sintering: Towards a facile synthetic route, robust thermal performance, and high-power solid state laser lighting[J]. Journal of the European Ceramic Society, 2018, 38(1): 343-347.

[19] Y. Zhang, Y. Liang, Y. Zhang, et al. High color rendering index composite phosphor-in glass for high-power white laser lighting[J]. Journal of the European Ceramic Society, 2021, 41(9): 4915-4923.

[20] Y. Zhou, W. Zhuang, Y. Hu, et al. Cyan-Green Phosphor $(Lu_2M)(Al_4Si)O_{12}:Ce^{3+}$ for High-Quality LED Lamp: Tunable Photoluminescence Properties and Enhanced Thermal Stability[J]. Inorg Chem, 2019, 58(2): 1492-1500.

[21] C Ma, F Tang, J Chen, et al. Spectral, energy resolution properties and green-yellow LEDs applications of transparent $Ce^{3+}:Lu_3Al_5O_{12}$ ceramics[J]. Journal of the European Ceramic Society, 2016, 36(16): 4205-4213.

[22] J Xu, J Wang, Y Gong, et al. Investigation of an LuAG:Ce translucent ceramic synthesized via spark plasma sintering: Towards a facile synthetic route, robust thermal performance, and high-power solid state laser lighting[J]. Journal of the European Ceramic Society, 2018, 38(1): 343-347.

[23] Y. L. Zhang, S. Hu, Z. J. Wang, et al. Pore-existing $Lu_3Al_5O_{12}$: Ce ceramic phosphor:an efficient green color converter for laser light source[J]. J. Lumin, 2018, 197(5): 331-334.

[24] Z. W. Hu, X. P. Chen, H. H. Chen, et al. Suppression of the slow scintillation component of $Pr:Lu_3Al_5O_{12}$ transparent ceramics by increasing Pr concentration[J]. J Lumin, 2019, 210(6): 14-20.

[25] A. Ikesue, I. Furusato, K. Kamata. Fabrication of polycrystalline, transparent YAG ceramics by a solid-state reaction method[J]. Journal of the American Ceramic Society, 1995, 78(1): 225-228.

[26] S. H. Lee, E. R. Kupp, A. J. Stevenson, et al. Hot isostatic pressing of transparent Nd:YAG

ceramics[J] Journal of the American Ceramic Society, 2009, 92(7): 1456-1463.

[27] X. P. Chen, Z. W. Hu, J. W. Dai, et al. Fabrication and optical properties of cerium doped $Lu_3Ga_3Al_2O_{12}$ scintillation ceramics[J]. Opt Mater, 2018, 85(11): 121-126.

[28] I. Milisavljevic, M. Pitcher, J. Q. Li, et al. Crystallization of glass materials into transparent optical ceramics[J]. International Materials Reviews, 2022, 68(6): 648-676.

[29] A. Rosenflanz, M. Frey, B. Endres, et al. Bulk glasses and ultrahard nanoceramics based on alumina and rare-earth oxides[J]. Nature, 2004, 430(7001): 761-764.

[30] M. Allix, S. Alahraché, F. Fayon, et al. Highly transparent $BaAl_4O_7$ polycrystalline ceramic obtained by full crystallization from glass[J]. Advanced Materials, 2012, 24(41): 5570-5575.

[31] S Alahrache, K Saghir, S Chenu, et al. Perfectly transparent $Sr_3Al_2O_6$ polycrystalline ceramic elaborated from glass crystallization[J]. Chem Mat, 2013, 25(20): 4017-4024.

[32] K. Al Saghir, S. Chenu, M. Allix, et al. Transparency through structural disorder a new concept for innovative transparent ceramics[J]. Chem Mater, 2015, 27(2): 508-514.

[33] X G Ma, X Y Li, J Q Li, et al. Pressureless glass crystallization of transparent yttrium aluminum garnet-based nanoceramics[J]. Nature Communications, 2018, 9(1): 1175.

[34] B.R. Johnson, W.M. Kriven. Crystallization kinetics of yttrium aluminum garnet ($Y_3Al_5O_{12}$)[J]. Journal of Materials Research, 2001, 16(6): 1795-1805.

[35] G. He, L. Mei, L. Wang, et al. Synthesis and luminescence properties of nano-/microstructured $Y_3Al_5O_{12}:Ce^{3+}$ microspheres by controlled glass crystallization[J]. Crystal Growth & Design, 2011, 11(12): 5355-5361.

[36] A. Prnov, A. Plsko, J. Valúchov, et al. Crystallization kinetics of glass microspheres with yttrium aluminium garnet (YAG) composition[J]. Journal of Thermal Analysis and Calorimetry, 2017, 131(2): 1115-1123.

[37] Zhang Y, Ma X, Li X, et al. Crystallization kinetics of Al_2O_3-26mol%Y_2O_3 glass and full crystallized transparent $Y_3Al_5O_{12}$-based nanoceramic[J]. Journal of the European Ceramic Society, 2021, 41(2): 1557-1563.

[38] H.E. Kissinger. Variation of peak temperature with heating rate in differential thermal

analysis[J]. Journal of Research of the National Bureau of Standards, 1956, 57(4): 217-221.

[39] G. Gupta, S. Balaji, K. Biswas, et al. Mid-IR transparent TeO_2-TiO_2-La_2O_3 glass and its crystallization behavior for photonic applications[J]. Journal of the American Ceramic Societ, 2018, 101(9): 3900-3916.

[40] P. Karmakar, A.K. Subudhi, K. Biswas, et al. Crystallization kinetics analysis of BaF_2 and $BaGdF_5$ nanocrystals precipitated from oxyfluoride glass systems: a comparative study[J]. Thermochim Acta, 2015, 610(20): 1-9.

[41] D.W. Henderson. Thermal analysis of non-isothermal crystallization kinetics in glass forming liquids[J]. Journal of Non-Crystalline Solids, 1979, 30(3): 301-315.

[42] W. Zhu, H. Jiang, H. Zhang, et al. Effect of TiO_2 and CaF_2 on the crystallization behavior of Y_2O_3-Al_2O_3-SiO_2 glass ceramics[J]. Ceram. Int, 2018, 44(6): 6653-6658.

[43] Y. Bai, L. Peng, Q. Zhu, et al. Non-isothermal crystallization kinetics of stoichiometric lithium disilicate-based glasses with Al_2O_3 additives[J]. Journal of Non-Crystalline Solids, 2016, 445(15): 116-122.

[44] J.A. Augis, J.E. Bennett. Calculation of the Avrami parameters for heterogeneous solid state reactions using a modification of the Kissinger method[J]. Journal of Thermal Analysis and Calorimetry, 1978, 13(2): 283-292.

[45] T. Ozawa. A new method of analyzing thermogravimetric data[J]. Bulletin of the Chemical Society of Japan, 1965, 38(11): 1881-1886.

[46] T. Ozawa, Kinetics of non-isothermal crystallization[J]. Polymer, 1971, 12(3): 150-158.

[47] K. Matusita, S. Sakka. Kinetic study of crystallization of glass by differential thermal analysis-criterion on application of Kissinger plot[J]. Journal of Non-Crystalline Solids, 1980, 38(2): 741-746.

[48] G Gupta, S Balaji, K Biswas, et al. Mid- IR transparent TeO_2-TiO_2-La_2O_3 glass and its crystallization behavior for photonic applications[J]. Journal of the American Ceramic Society, 2018, 101(9): 3900-3916.

[49] A L Patterson. The Scherrer formula for X-ray particle size determination[J]. Physical Review,

1939, 56(10): 978-982.

[50] W C Oliver, G M Pharr. An improved technique for determining hardness and elastic modulus using load and displacement sensing indentation experiments[J]. Journal of Materials Research, 2011, 7(6): 1564-1583.

[51] T. Irifune, K. Kawakami, T. Arimoto, et al. Pressureinduced nano-crystallization of silicate garnets from glass[J]. Nature Communcations, 2016, 7(1): 1-7.

Supporting Information

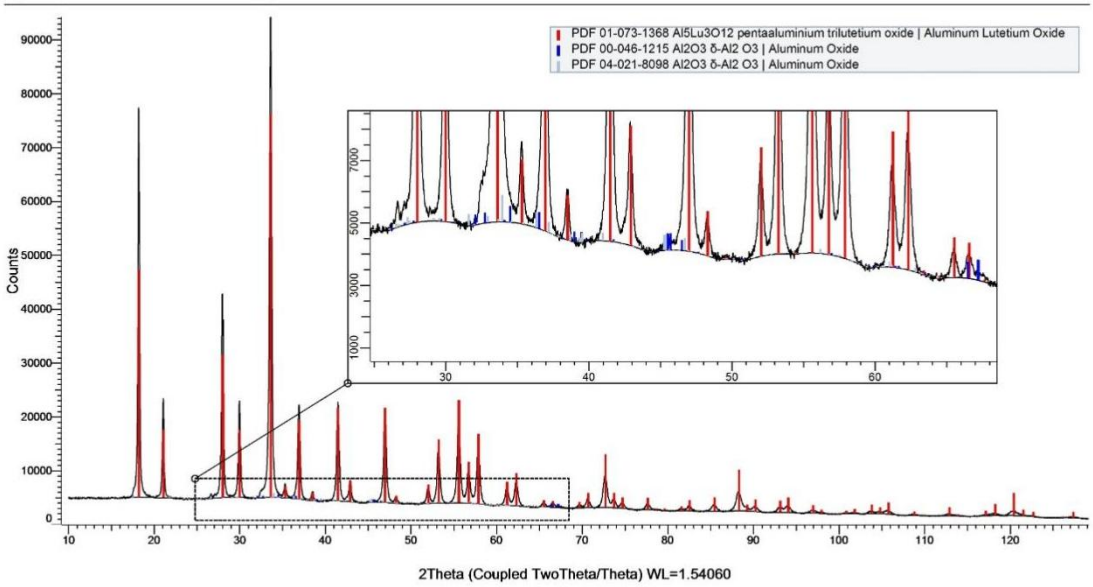

Figure S1. High-resolution XRPD pattern of ceramic sample crystallized from ALu28 glass at 1000 ℃ for 2 h.